

 Open access • Journal Article • DOI:10.1038/S41558-018-0346-Z

## Contrasting responses of autumn-leaf senescence to daytime and night-time warming — [Source link](#)

[Chaoyang Wu](#), [Xiaoyue Wang](#), [Huanjiong Wang](#), [Philippe Ciais](#) ...+15 more authors

**Institutions:** [Chinese Academy of Sciences](#), [Centre national de la recherche scientifique](#), [Spanish National Research Council](#), [Boston University](#) ...+9 more institutions

**Published on:** 01 Dec 2018 - [Nature Climate Change](#) (Nature Publishing Group)

Related papers:

- [Climate change, phenology, and phenological control of vegetation feedbacks to the climate system](#)
- [Leaf onset in the northern hemisphere triggered by daytime temperature](#)
- [Delayed autumn phenology in the Northern Hemisphere is related to change in both climate and spring phenology.](#)
- [Plant phenology and global climate change: Current progresses and challenges](#)
- [Declining global warming effects on the phenology of spring leaf unfolding.](#)

Share this paper:    

View more about this paper here: <https://typeset.io/papers/contrasting-responses-of-autumn-leaf-senescence-to-daytime-34dnp95v3s>

This is the accepted version of the article: Wu, C. et al. *Contrasting responses of autumn-leaf senescence to daytime and night-time warming* in Nature climate change (Ed. Nature publishing), vol. 8 (Dec. 2018), p. 1092-1096.

Available at: DOI [10.1038/s41558-018-0346-z](https://doi.org/10.1038/s41558-018-0346-z)

This version is published under a “All rights reserved” license.

1 **Contrasting responses of autumn leaf senescence to daytime**  
2 **and nighttime warming**

3 **Chaoyang Wu<sup>1,2\*</sup>, Xiaoyue Wang<sup>1,2</sup>, Huanjiong Wang<sup>1,2\*</sup>, Philippe Ciais<sup>3</sup>, Josep**  
4 **Peñuelas<sup>4,5</sup>, Ranga B. Myneni<sup>6</sup>, Ankur R. Desai<sup>7</sup>, Christopher M. Gough<sup>8</sup>, Alemu**  
5 **Gonsamo<sup>9</sup>, Andrew T. Black<sup>10</sup>, Rachhpal S. Jassal<sup>10</sup>, Weimin Ju<sup>11</sup>, Wenping Yuan<sup>12</sup>,**  
6 **Yongshuo Fu<sup>13</sup>, Miaogen Shen<sup>14</sup>, Shihua Li<sup>15</sup>, Ronggao Liu<sup>16</sup>, Jing M. Chen<sup>9</sup>,**  
7 **Quansheng Ge<sup>1,2\*</sup>**

8 *1. The Key Laboratory of Land Surface Pattern and Simulation, Institute of Geographical*  
9 *Sciences and Natural Resources Research, Chinese Academy of Sciences, Beijing*  
10 *100101, China;*

11 *2. University of the Chinese Academy of Sciences, Beijing 100049, China;*

12 *3. Laboratoire des Sciences du Climat et de l'Environnement, IPSL-LSCE CEA CNRS*  
13 *UVSQ, 91191, Gif sur, Yvette, France;*

14 *4. CSIC, Global Ecology Unit CREAM-CSIC-UAB, Bellaterra, Barcelona 08193, Catalonia,*  
15 *Spain.*

16 *5. CREAM, Cerdanyola del Valles, Barcelona 08193, Catalonia, Spain;*

17 *6. Department of Earth and Environment, Boston University, 685 Commonwealth Avenue,*  
18 *Boston, MA 02215, USA;*

19 *7. Department of Atmospheric and Oceanic Sciences, University of Wisconsin-Madison,*  
20 *Madison, WI, USA;*

21 *8. Department of Biology, Virginia Commonwealth University, Richmond, VA 23284-2012,*  
22 *USA;*

23 *9. Department of Geography and Planning, University of Toronto, 100 St. George St.,*  
24 *Toronto, ON, M5S 3G3, Canada;*

25 *10. Faculty of Land and Food Systems, University of British Columbia, Vancouver, BC,*  
26 *Canada;*

27 *11. International Institute for Earth System Science, Nanjing University, 22 Hankou Road,*  
28 *Nanjing, 210093, China;*

29 *12. School of Atmospheric Sciences, Center for Monsoon and Environment Research,*  
30 *Sun Yat-Sen University, Guangzhou 510275, China;*

31 *13. College of Water Sciences, Beijing Normal University, 100875, Beijing, China;*

32 *14. CAS Center for Excellence in Tibetan Plateau Earth Sciences, Beijing 100101, China;*

33 *15. School of Resources and Environment, University of Electronic Science and*  
34 *Technology of China, Chengdu 611731, China;*

35 *16. State key Laboratory of Resources and Environmental Information system, Institute of*  
36 *Geographic Sciences and Natural Resources Research, CAS, Beijing 100101, China*

37

38 **\*Corresponding authors:** C Wu (wucy@igsnr.ac.cn), H Wang (wanghj@igsnr.ac.cn)  
39 and Q Ge (geqs@igsnr.ac.cn).

40 Plant phenology is a sensitive indicator of climate change<sup>1-4</sup>, and plays a significant role in  
41 regulating carbon uptake by plants<sup>5-7</sup>. Previous studies have focused on spring leaf-out by  
42 daytime temperature and the onset of snowmelt time<sup>8-9</sup>, but the drivers controlling leaf  
43 senescence date (LSD) in autumn remain largely unknown<sup>10-12</sup>. Using long-term ground  
44 phenological records (14536 time series since the 1900s) and satellite greenness  
45 observations dating back to the 1980s, we show that rising preseason maximum daytime  
46 ( $T_{\text{day}}$ ) and minimum nighttime ( $T_{\text{night}}$ ) temperatures had contrasting effects on the timing of  
47 autumn LSD in the Northern Hemisphere ( $>20^{\circ}\text{N}$ ). If higher  $T_{\text{day}}$  leads to an earlier or later  
48 LSD, an increase in  $T_{\text{night}}$  systematically drives LSD to occur oppositely. Contrasting  
49 impacts of daytime and nighttime warming on drought stress may be the underlying  
50 mechanism. A new LSD model considering these opposite effects improved autumn  
51 phenology modeling, and predicted an overall earlier autumn LSD by the end of this  
52 century compared with traditional projections. These results challenge the notion of  
53 prolonged growth under higher autumn temperatures, suggesting instead that leaf  
54 senescence in the Northern Hemisphere will begin earlier than currently expected,  
55 causing a positive climate feedback.

56

57 Climate change over the last several decades has modified the dates of plant flowering,  
58 leaf emergence, growth stages, and senescence, collectively termed phenology<sup>13</sup> with  
59 substantial ecological and environmental consequences<sup>4</sup>. Both observations and model  
60 simulations have found that air temperature has a positive influence on the onset of plant  
61 growth in the Northern Hemisphere (NH), e.g., higher spring temperature triggers earlier

62 leaf-out and flowering dates and hence extends the growing season<sup>8,14-15</sup>. In contrast to  
63 those extensive research efforts on spring phenology, autumn phenology, particularly leaf  
64 senescence date (LSD), is more challenging to understand, and has not received  
65 sufficient attention<sup>16,17</sup>, while also serving as an important indicator of changing foliar  
66 physiological properties. Yet, autumn phenology may be as important as spring in  
67 regulating the interannual variability of carbon balance<sup>7</sup>.

68

69 LSD has been occurring later in most regions over the last few decades<sup>18</sup>, but providing  
70 an explanation for this change is difficult<sup>9</sup>. An increase in global temperature is assumed  
71 to be a driver of LSD trends<sup>19</sup>, but studies indicated that the contribution of temperature to  
72 LSD variability is low, especially compared to spring phenology<sup>20,21</sup>. We argue that  
73 ignoring the asymmetric effects<sup>22</sup> of daytime maximum temperature ( $T_{\text{day}}$ ) versus  
74 nighttime minimum temperature ( $T_{\text{night}}$ ) and their differing impacts on LSD, contributes to  
75 the reported overall low contribution of temperature to LSD variability. To test this, we  
76 used measured and gridded preseason (defined as months from June to LSD)  $T_{\text{day}}$  and  
77  $T_{\text{night}}$  in the NH, together with LSD data from three different datasets: (a) long-term  
78 phenological observations at ground sites from 14536 time series since the 1900s (Fig.  
79 S1), (b) the latest third generation of the Normalized Difference Vegetation Index (NDVI,  
80 GIMMS3g.v1) for 1982-2015, and (c) NDVI and enhanced vegetation index (EVI) from the  
81 Moderate Resolution Imaging Spectroradiometer (MODIS) products for 2001-2015.

82

83 Preseason forcing had a better predictive strength on LSD than either summer or autumn

84 climate forcing alone (Fig. S2). Because pre-season  $T_{\text{day}}$  and  $T_{\text{night}}$  were highly correlated,  
85 we used a partial correlation to remove the effects of  $T_{\text{night}}$  and of precipitation and  
86 radiation (similarly for  $T_{\text{night}}$ ) to investigate the response of LSD to  $T_{\text{day}}$ . Correlations were  
87 classified into four types, (A)  $T_{\text{day}}^+T_{\text{night}}^+$ , (B)  $T_{\text{day}}^-T_{\text{night}}^-$ , (C)  $T_{\text{day}}^+T_{\text{night}}^-$  and (D)  $T_{\text{day}}^-T_{\text{night}}^+$ ,  
88 where  $T^+$ ,  $T^-$  represent positive and negative partial correlation coefficient of  $T$  with LSD.

89

90 Overall, all three datasets suggested that the onset of autumn LSD responded oppositely  
91 to  $T_{\text{day}}$  and  $T_{\text{night}}$ . The proportions of ground sites of Types A and B were significantly lower  
92 than those of Type C and D (Fig. 1a). More significant  $R$  values for both  $T_{\text{day}}$  and  $T_{\text{night}}$   
93 were found within Types C and D, with only two and one records out of 2231 time series  
94 having significant  $R$  within Type A and B, respectively. These results from ground sites  
95 are consistent with those for the two satellite greenness products (Fig. 1b, c). Types C and  
96 D together accounted for 83.7 and 80.0% for GIMMS3g and MODIS pixels, respectively.  
97 Only 0.8 and 1.5% of the pixels had the same sign of response of LSD to  $T_{\text{day}}$  or  $T_{\text{night}}$  (i.e.  
98 significant pixels for Types A+B) for GIMMS3g and MODIS, respectively. The GIMMS3g  
99 dataset contained different fractions of Types C and D (45.6% vs. 38.1%), but the  
100 compositions of Type C and D in GIMMS3g (i.e., contrasting effects of night and day  
101 temperatures) became more consistent with the MODIS results when the overlapping  
102 periods between the two sensors is considered (Figs. S3-4). More details on the fractions  
103 of the four correlation types for different vegetation types are provided in Figs. S5-6.

104

105 **Figure 1 Frequency of the partial correlation coefficient ( $R$ ) between leaf senescence date**

106 **(LSD) and daytime ( $T_{\text{day}}$ ), nighttime ( $T_{\text{night}}$ ) temperatures.** (a) Data for 14536 time series of  
107 ground sites, (b) the GIMMS3g dataset for 1982-2015, and (c) the MODIS product for  
108 2001-2015.  $T^+$ ,  $T^-$  represent positive and negative partial correlation coefficient of  $T$  with  
109 LSD. Significance was set at  $P < 0.05$ .

110

111 The satellite greenness products also allowed us to evaluate spatial patterns of LSD  
112 changes in response to variations in  $T_{\text{day}}$  and  $T_{\text{night}}$  (Fig. 2). For the GIMMS3g data, higher  
113  $T_{\text{day}}$  was associated with a delayed LSD for 10.7% of the pixels (mostly boreal regions)  
114 and with an earlier LSD for 7.5% of the pixels (central North America, borders of Eurasia  
115 and central China).  $T_{\text{night}}$  had evident opposite influences on LSD than  $T_{\text{day}}$ . The patterns  
116 of opposite effects from  $T_{\text{day}}$  and  $T_{\text{night}}$  on LSD were highly spatially consistent in all  
117 regions where  $T_{\text{day}}$  and  $T_{\text{night}}$  were significantly correlated with LSD. Similar results were  
118 obtained with MODIS observations (Fig. 2b, d). LSD for approximately 20% all pixels was  
119 significantly correlated with  $T_{\text{day}}$ , of which 60.1 and 39.9% were negatively and positively  
120 correlated, respectively. The area where LSD was positively correlated with  $T_{\text{night}}$  was  
121 larger (9.4%) than the area with negative correlations (6.5%).

122

123 Vegetation grouped into Köppen-Geiger zones showed contrasting patterns between the  
124 effects of  $T_{\text{day}}$  and  $T_{\text{night}}$  on LSD (Fig. 2e, f). Type D was more widely distributed, while  
125 Type C was more common for continental climates. Monsoon-influenced but not  
126 extremely cold regions and mild climates also had higher proportions of Type C. Grouping  
127 these correlation types by vegetation types lead to similar results (Fig. 2g, h). In theory,

128 we would expect to find Type C more in wet vegetation types and Type D in dry types. The  
129 real world seems to show the same thing but still there could be many locations that do  
130 not neatly fall into that continuum and suggests additional mechanisms may work,  
131 probably adaption.

132

133 **Figure 2 Spatial distributions of the partial correlation coefficient (R) between leaf**  
134 **senescence date (LSD) and daytime ( $T_{\text{day}}$ ), nighttime ( $T_{\text{night}}$ ) temperatures.  $R^+$ ,  $R^-$**   
135 **represent positive and negative partial correlation coefficient of T with LSD. (a) LSD vs.**  
136  **$T_{\text{day}}$  for GIMMS3g, (b) LSD vs.  $T_{\text{day}}$  for MODIS, (c) LSD vs.  $T_{\text{night}}$  for GIMMS3g, and (d)**  
137 **LSD vs.  $T_{\text{night}}$  for MODIS. (e), (f), represent distributions of correlation types in**  
138 **Köppen-Geiger climatic classification using GIMMS3g and MODIS, respectively. (g) and**  
139 **(h) represent distributions of correlation types for vegetation types (see Methods) using**  
140 **GIMMS3g and MODIS, respectively. Significance was set at  $P < 0.05$ .**

141

142 Our results suggest that ecological trade-offs, particularly those driven by regional  
143 differences in water stress, may underlie the contrasting relationships between LSD and  
144  $T_{\text{day}}$  and  $T_{\text{night}}$ . Type C was mostly found in humid regions where water is a less limiting  
145 factor for plant growth. In these cases, a higher  $T_{\text{day}}$ , in the likely absence of severe water  
146 stress, benefits photosynthesis while elevated  $T_{\text{night}}$  increases nighttime leaf respiration.

147

148 Explanations for the prevalence of Type D relations in dry regions are more complicated.

149 The Standardized Precipitation Evapotranspiration Index (SPEI)<sup>23</sup>, an indicator of drought



150 stress, accounted for the contrasting effects of increases in  $T_{\text{day}}$  and  $T_{\text{night}}$  on LSD for Type  
151 D (Fig. 3). Partial correlation data indicate that increased  $T_{\text{day}}$  is negatively correlated with  
152 SPEI (Fig. 3a), a stronger sensitivity to drought in dry regions that negatively affects plant  
153 growth and consequently leads to an earlier LSD. In contrast, we found that an increase in  
154  $T_{\text{night}}$  is associated with a higher SPEI, that is, wetter conditions, and arguably reduced  
155 water stress, which could extend the duration of photosynthesis and lead to delayed LSD  
156 (Fig. 3b). The latter mechanism is consistent with the generally positive partial correlation  
157 values between evapotranspiration (ET) and  $T_{\text{night}}$ , that is, more soil moisture being  
158 available for ET in the late season, and sustaining delayed LSD (Fig. 3f), and with studies  
159 showing that water stress accelerates leaf drop in dry ecosystems more so than in humid  
160 ecosystems<sup>24</sup>. The responses of radiation to  $T_{\text{day}}$  and  $T_{\text{night}}$  may also be viewed as a  
161 further evidence for the linkage between leaf senescence and plant water status to  
162 support the contrasting patterns (Fig. S7), given that a higher  $T_{\text{day}}$  was associated with  
163 stronger radiation and potentially a higher chance of water stress. These findings suggest  
164 that dry regions, in which Type D dominates, may be especially vulnerable to earlier onset  
165 of LSD if climate change reduces local precipitation and increases daytime evaporation  
166 with rising  $T_{\text{day}}$ .

167

168 Apart from physiological mechanisms relating to water stress, ecological processes may  
169 also contribute to these patterns. Warmer daytime versus nighttime temperature may  
170 have contrasting effects on different species since species adaptations lead to intrinsic  
171 differences in their timing of leaf emergence and senescence that are optimized to

172 maximize carbon gain and minimize water losses<sup>25-27</sup>. The ecosystem-scale responses of  
173 phenology reflects the scaled responses of ecological dynamics of multiple individual  
174 species gaining or losing a competitive advantage in a changing climate, or presenting an  
175 induced advantage as a result of land-use change and planting<sup>17,26</sup>. Recent results  
176 suggest that the magnitude of phenological change to effects by shifts in plant species  
177 composition may be similar as that by climate change<sup>27</sup>, and the autumn phenology may  
178 thus change accordingly.

179

180 **Figure 3 Partial correlation coefficient (R) between the Standardized Precipitation**  
181 **Evapotranspiration Index (SPEI), evapotranspiration (ET), and daytime ( $T_{\text{day}}$ ), nighttime**  
182 **( $T_{\text{night}}$ ) temperatures. (a) SPEI vs.  $T_{\text{day}}$  for GIMMS3g, (b) SPEI vs.  $T_{\text{night}}$  for GIMMS3g, (c)**  
183 **SPEI vs.  $T_{\text{day}}$  for MODIS, (d) SPEI vs.  $T_{\text{night}}$  for MODIS, (e) ET vs.  $T_{\text{day}}$  for MODIS, and (f)**  
184 **ET vs.  $T_{\text{night}}$  for MODIS. Significance was set at  $P < 0.05$ .**

185

186 We tested the implications of the observation analysis on future trends in autumn LSD by  
187 developing a weighted day-night-temperature growing-degree-day ( $DN_{\text{GDD}}$ ) algorithm  
188 incorporating these opposite changes in LSD to  $T_{\text{day}}$  and  $T_{\text{night}}$  (see Methods). The new  
189 model substantially improved LSD modeling (in terms of R (Figs. S8-10), RMSE (Figs.  
190 S11-13) and percentage of significant pixels (Figs. S14-15)) compared with the currently  
191 used threshold or GDD methods both for the overall dataset and for vegetation types.

192

193 Spatial patterns of improvements using MODIS and GIMMS3g were also investigated

194 (Figs. S16-17). The results from MODIS and the ground sites (Fig. S18) were more  
195 consistent with the new model, and the accuracy of the threshold method was much lower,  
196 so we used the coefficients from the MODIS data to predict LSD variability by the end of  
197 this century using traditional GDD and  $DN_{GDD}$  algorithms under two Representative  
198 Concentration Pathways (RCP) scenarios (RCP 4.5 and RCP 8.5) (Fig. S19, and Fig. 4).  
199  
200 LSD from the  $DN_{GDD}$  method was overall earlier than conventional predictions across  
201 Köppen-Geiger climatic classification types. Globally, LSD was earlier for about 68% of  
202 the terrestrial biosphere under RCP 4.5 and for about 70% under RCP 8.5. LSD was  
203 mostly later for central North America, western Russia, and southwestern China. Most  
204 vegetation types showed earlier LSD estimates under two RCP scenarios while the  
205 temperate grasslands were expected to have later senescence dates.

206

207

208 **Figure 4 Leaf senescence date (LSD) differences from the weighted**  
209 **day-night-temperature growing-degree-day ( $DN_{GDD}$ ) and traditional GDD**  
210 **( $LSD_{DN_{GDD}}-LSD_{GDD}$ ) models under two RCP scenarios. (a), (b), (c) represent**  
211  **$LSD_{DN_{GDD}}-LSD_{GDD}$  under RCP 4.5, and averages of differences for the Köppen-Geiger**  
212 **climatic classification, and vegetation types, respectively. (d), (e), (f) represent**  
213  **$LSD_{DN_{GDD}}-LSD_{GDD}$  under RCP 8.5, and averages of differences for the Köppen-Geiger**  
214 **climatic classification, and vegetation types, respectively.**

215

216 Climatic variability, particularly temperature, has driven phenological changes over the  
217 last several decades but has been challenging to predict. Our ability to predict autumn  
218 LSD is particularly limited. We are the first to report, using 14536 ground time series and  
219 more than 30 years of remotely sensed observations, the opposite responses of LSD to  
220 daytime and nighttime warming, providing a new perspective to account for the previous  
221 low estimation accuracy of autumn LSD when relying solely on mean temperature. A  
222 model based on mean temperature cannot correctly predict LSD changes, because LSD  
223 responds to  $T_{\text{day}}$  and  $T_{\text{night}}$  in opposite directions. Our results also provide a perspective to  
224 account for the carry-over effects between spring and autumn phenology, i.e. the start and  
225 end of a growing season always move in the same direction<sup>28</sup>. An earlier start of a season  
226 is mainly triggered by higher spring temperatures, with increased growth depleting soil  
227 water<sup>29</sup>, which is then associated with autumn drought, inducing a reduction in growth and  
228 consequently leading to an earlier end to the growing season<sup>30</sup>.

229

230 Our improvement in modeling autumn phenology is a strong and convincing evidence for  
231 the value of incorporating daytime and nighttime temperatures in terrestrial models, rather  
232 than mean temperature alone. The application of this model projects an overall earlier  
233 than currently expected start of autumn senescence in the NH by the end of this century,  
234 particularly in dry regions. The earlier data of autumn senescence may be a potentially  
235 unrecognized positive feedback to climate change and consequently a weakening in the  
236 capability of terrestrial carbon uptake.

237

238 **Acknowledgments:** This work was funded by the Strategic Priority Research Program of  
239 the Chinese Academy of Sciences (XDA19040103), International Cooperation and  
240 Exchange Programs of National Science Foundation of China  
241 (Sino-German, 41761134082), National Natural Science Foundation of China (41522109)  
242 and the key Research Program of Frontier Sciences, CAS (QYZDB-SSW-DQC011). J.P.  
243 and P.C. were funded by European Research Council Synergy grant  
244 ERC-SyG-2013-610028 IMBALANCE-P. A.R.D. acknowledges support from the Ned P  
245 Smith Professorship of Climatology, University of Wisconsin-Madison.

246

247 **Contributions:** C.W., H.W. and Q.G. designed the research. C.W. wrote the first draft of  
248 the paper. J.P. and C.P. extensively revised the writing. H.W. performed the site model  
249 simulations. X.W. performed remote sensing model simulations. All the authors  
250 contributed to writing the paper.

251

252 **Correspondence and requests for materials should be addressed C.W.**

253

254 **Competing interests:** The authors declare no competing financial interests.

255

## 256 **References**

257 1. Fu, Y. H., et al (2015). Declining global warming effects on the phenology of spring leaf  
258 unfolding. Nature, 526, 104-107.

259 2. Xia, J., et al (2015). Joint control of terrestrial gross primary productivity by plant

260 phenology and physiology. *Proceedings of the National Academy of Sciences*, 112,  
261 2788-2793.

262 3. Buitenwerf, R., et al (2015). Three decades of multi-dimensional change in global leaf  
263 phenology. *Nature Climate Change*, 5, 364.

264 4. Peñuelas, J., & Filella, I. (2009). Phenology feedbacks on climate change. *Science*, 324,  
265 887-888.

266 5. Richardson, A. D., et al (2013). Climate change, phenology, and phenological control of  
267 vegetation feedbacks to the climate system. *Agricultural and Forest Meteorology*, 169,  
268 156-173.

269 6. Keenan, T.F., et al. (2014) Net carbon uptake has increased through warming-induced  
270 changes in temperate forest phenology. *Nature Climate Change*, 4, 598-604.

271 7. Wu, C., et al (2013). Interannual variability of net ecosystem productivity in forests is  
272 explained by carbon flux phenology in autumn. *Global Ecology and Biogeography*, 22,  
273 994-1006.

274 8. Piao, S., et al (2015). Leaf onset in the northern hemisphere triggered by daytime  
275 temperature. *Nature communications*, 6, doi:10.1038/ncomms7911.

276 9. Pulliainen, J., et al. (2017). Early snowmelt significantly enhances boreal springtime  
277 carbon uptake. *Proceedings of the National Academy of Sciences*, 114, 11081-11086.

278 10. Liu, Q., et al. (2016). Delayed autumn phenology in the Northern Hemisphere is  
279 related to change in both climate and spring phenology. *Global change biology*, 22,  
280 3702-3711.

281 11. Keenan, T.F., & Richardson, A. D. (2015). The timing of autumn senescence is

282 affected by the timing of spring phenology: implications for predictive models. *Global*  
283 *Change Biology*, 21, 2634-2641.

284 12. Gill, A.L., et al (2015). Changes in autumn senescence in northern hemisphere  
285 deciduous trees: a meta-analysis of autumn phenology studies. *Annals of botany*, 116,  
286 875-888.

287 13. Myneni, R.B., et al (1997). Increased plant growth in the northern high latitudes from  
288 1981 to 1991. *Nature*, 386, 698-702.

289 14. Suni, T., et al (2003). Air temperature triggers the recovery of evergreen boreal forest  
290 photosynthesis in spring. *Global Change Biology*, 9, 1410–1426.

291 15. Richardson, A.D., et al (2012). Terrestrial biosphere models need better  
292 representation of vegetation phenology: results from the North American Carbon Program  
293 Site Synthesis. *Global Change Biology*, 18, 566-584.

294 16. Gallinat, A.S., et al (2015). Autumn, the neglected season in climate change  
295 research. *Trends in Ecology & Evolution*, 30, 169-176.

296 17. Walther, G.R., et al (2002). Ecological responses to recent climate  
297 change. *Nature*, 416, 389-395.

298 18. Zhu, W., et al (2012). Extension of the growing season due to delayed autumn over  
299 mid and high latitudes in North America during 1982–2006. *Global Ecology and*  
300 *Biogeography*, 21, 260-271.

301 19. Garonna, I., et al (2014). Strong contribution of autumn phenology to changes in  
302 satellite-derived growing season length estimates across Europe (1982–2011). *Global*  
303 *Change Biology*, 20, 3457-3470.

304 20. Yang, Y., et al (2015). Changes in autumn vegetation dormancy onset date and the  
305 climate controls across temperate ecosystems in China from 1982 to 2010. *Global change*  
306 *biology*, 21, 652-665.

307 21. Jeong, S. J., et al (2011). Phenology shifts at start vs. end of growing season in  
308 temperate vegetation over the Northern Hemisphere for the period 1982–2008. *Global*  
309 *Change Biology*, 17, 2385-2399.

310 22. Peng, S., et al (2013). Asymmetric effects of daytime and night-time warming on  
311 Northern Hemisphere vegetation. *Nature*, 501, 88-92.

312 23. Beguería, S., et al (2014). Standardized precipitation evapotranspiration index (SPEI)  
313 revisited: parameter fitting, evapotranspiration models, tools, datasets and drought  
314 monitoring. *International Journal of Climatology*, 34, 3001-3023.

315 24. Meng, T.T, et al (2009). Plant morphometric traits and climate gradients in northern  
316 China: a meta-analysis using quadrat and flora data. *Annals of Botany*, 104,1217-1229.

317 25. Prasad, V.K., et al. (2007). Spatial patterns of vegetation phenology metrics and  
318 related climatic controls of eight contrasting forest types in India - analysis from remote  
319 sensing datasets. *Theoretical and Applied Climatology*, 89:95-107

320 26. Peñuelas J., et al. (2013). Evidence of current impact of climate change on life: a walk  
321 from genes to the biosphere. *Global Change Biology*,19, 2303-2338.

322 27. Wolf, A.A., et al. (2017). Flowering phenology shifts in response to biodiversity  
323 loss. *Proceedings of the National Academy of Sciences*, 114, 3463-3468.

324 28. Fu, Y. S., et al (2014). Variation in leaf flushing date influences autumnal senescence  
325 and next year's flushing date in two temperate tree species. *Proceedings of the National*



326 Academy of Sciences, 111, 7355-7360.

327 29. Wolf, S., et al (2016). Warm spring reduced carbon cycle impact of the 2012 US  
328 summer drought. Proceedings of the National Academy of Sciences, 113, 5880-5885.

329 30. Peñuelas, J., et al (2017). Shifting from a fertilization-dominated to a  
330 warming-dominated period. Nature Ecology & Evolution, 1, 1438-1445.

331

## 332 **Methods**

### 333 **1. Phenological observation data**

334 We used observations of leaf senescence date (LSD) from three independent  
335 phenological datasets.

336 1) The Pan European Phenological Database (PEP725; <http://www.pep725.eu/>), an  
337 open-access database with long term plant phenological observations (since 1868)  
338 from 19608 sites and 78 species across 25 European countries.

339 2) The China Phenological Observation Network (CPON), with data since 1963 for >100  
340 species at 42 sites across China.

341 3) LSD data for two tree species (*Acer palmatum* and *Ginkgo biloba*) at 54 meteorological  
342 stations in South Korea for 1989-2007<sup>31</sup>.

343 The definitions of LSD notably differ among the datasets. LSD for the PEP725, CPON,  
344 and Korean datasets is defined as the date when 50, 90, and 20% of the tree leaves,  
345 respectively, change color from green to red or yellow. We removed outliers using the  
346 methods<sup>32</sup> to exclude potential biases and inadequate degrees of freedom and focused on  
347 time series with at least 15 years of records for 1900-2015. We thus analyzed 14536 LSD

348 time series for 24 species (Table S1).

349

## 350 **2. LSD derived from satellite data**

351 LSD in the Northern Hemisphere was determined using two satellite-derived  
352 vegetation indices, the Normalized Difference Vegetation Index (NDVI) and the Enhanced  
353 Vegetation Index (EVI)<sup>33</sup>. Both NDVI and EVI are direct indicators of vegetation growth and  
354 have been widely applied for investigating vegetation phenology<sup>34</sup>. We used two datasets  
355 to reduce the uncertainties caused by a single data source: GIMMS NDVI third-generation  
356 (NDVI3g) data derived from the Advanced Very High Resolution Radiometer (AVHRR)  
357 and NDVI and EVI derived from the Moderate Resolution Imaging Spectroradiometer  
358 (MODIS). The GIMMS NDVI3g data have a spatial resolution of 1/12°, a half-month  
359 interval, and a 34-year time span (1982-2015). The MODIS 16-day composite product  
360 MOD13C1 (Collection 6) includes both NDVI and EVI with a 0.05° resolution for  
361 2001-2015.

362 We eliminated the impacts of areas with sparse vegetation on the results by first  
363 excluding pixels with annual NDVI <0.1 or annual EVI <0.08<sup>35</sup>. A Savitzky-Golay filter was  
364 then used to smooth the NDVI (EVI) time series<sup>36</sup>. We then estimated LSD using two  
365 methods.

366 The first method was a dynamic-threshold approach, which uses an annually defined  
367 threshold for each pixel based on the NDVI ratio:

$$368 \quad NDVI_{ratio} = (NDVI - NDVI_{min}) / (NDVI_{max} - NDVI_{min}) \quad (1)$$

369 where NDVI is the daily NDVI and  $NDVI_{max}$  and  $NDVI_{min}$  are the annual daily maximum

370 and minimum of NDVIs. The  $NDVI_{ratio}$  ranges from 0 to 1. LSD is determined when  
371  $NDVI_{ratio}$  decreases to 0.5 in autumn<sup>37,38</sup>.

372 The second method was based on a series of piecewise logistic functions. The NDVI  
373 time series were first divided into two sections by the maximum daily NDVI in each year,  
374 and a double logistic function was applied to fit each section<sup>39</sup>:

$$375 \quad y(t) = a_1 + (a_2 - a_7 t) \left[ \frac{1}{1 + e^{(a_3 - t) / a_4}} - \frac{1}{1 + e^{(a_5 - t) / a_6}} \right] \quad (2)$$

376 LSD was then defined as the time when the curvature changing rate reached its last  
377 local maximum value.

378 For GIMMS3g data, we calculated LSD using NDVI from both the dynamic-threshold  
379 approach and the piecewise logistic function method. Since MODIS sensor provides EVI,  
380 we further used EVI-based logistic function method to derive LSD. To sum up, for  
381 GIMMS3g data, average LSD from threshold and logistic function method were used, and  
382 for MODIS, an additional LSD from EVI-based logistic function method was used (not for  
383 MODIS NDVI data).

384 At high latitudes (or elevations), snow cover is important for regional climate and  
385 arrives early in autumn and potentially masking evergreen vegetation. However, we  
386 suggested that using a Savitzky-Golay filter could solve the noise from a "sudden" change  
387 in the time series of NDVI due to snow<sup>36</sup>. In particular, a study showed that snowfall had  
388 little influence on determining EOS in western Arctic Russia<sup>41</sup>. For high elevations, our  
389 previous analysis on Tibetan Plateau showed that for more than 98% of regions snow  
390 happened later than LSD<sup>42</sup>.

391

392 **3. Climatic data**

393 We used the CRU-TS 4.00 dataset with a spatial resolution of  $0.5^{\circ} \times 0.5^{\circ}$  for  
394 1901-2015. We extracted monthly data for  $T_{\max}$ ,  $T_{\min}$ ,  $T_{\text{mean}}$ , precipitation, and cloud cover  
395 from this dataset for analyzing LSD from in-situ observations and the two remote sensing  
396 data. We modeled past and future LSD by temperature by acquiring daily gridded data for  
397 maximum and minimum temperature with a spatial resolution of  $0.5^{\circ}$  from NOAA Earth  
398 System Research Laboratory Physical Sciences Division for 1982-2015. We used daily  
399  $T_{\max}$  and  $T_{\min}$  simulated by the CCSM 4 model under two climatic scenarios (RCP4.5 and  
400 RCP8.5) for future climatic data (2081-2100). These data were from an open-access  
401 database of the Coupled Model Intercomparison Project Phase 5.

402

403 **4. Analyses**

404 We used partial correlation analyses to determine the responses of LSD to  $T_{\text{day}}$  and  
405  $T_{\text{night}}$ . The reason is that directly correlating LSD to  $T_{\text{day}}$  would give misleading results  
406 since  $T_{\text{night}}$  is a confounding variable that is numerically related to both LSD and  $T_{\text{day}}$ ,  
407 violating independence of variables in multiple correlation tests. Thus, using the partial  
408 correlation between LSD and  $T_{\text{day}}$  will measure the degree of association with the effect of  
409 a set of controlling random variables removed (e.g.,  $T_{\text{night}}$ , precipitation, radiation), given  
410 that these factors have shown strong influences on LSD<sup>10, 20</sup>. Since Echer and Silva (2014)  
411 demonstrated that clouds are the main atmospheric factor modulating the surface  
412 incidence of solar radiation<sup>43</sup>, cloud cover data was used to model the effect of radiation  
413 on LSD, as similarly conducted in previous analyses<sup>8</sup>. Correlations were classified into

414 four types, (A)  $T_{\text{day}}^+T_{\text{night}}^+$ , (B)  $T_{\text{day}}^-T_{\text{night}}^-$ , (C)  $T_{\text{day}}^+T_{\text{night}}^-$  and (D)  $T_{\text{day}}^-T_{\text{night}}^+$ , where  $T^+$ ,  $T^-$   
415 represent positive and negative partial correlation coefficient of  $T$  with LSD. An  $R$  of at  
416 least 0.514 for MODIS is required for the significance test ( $p = 0.05$ ), but this value  
417 decreases to 0.339 for the longer GIMMS3g data. These analyses were investigated for  
418 both Köppen-Geiger climatic classifications and vegetation types (Table S2<sup>40</sup>). Crops  
419 were excluded because their signal may result from changes in cropping or harvest cycles,  
420 rather than from climate change. Furthermore, since at low latitudes plant phenology of  
421 tropical and subtropical areas responds to other factors than temperature, regions with  
422 latitudes  $< 20^\circ$  N were also excluded.

423 Current phenology algorithms in most terrestrial-biosphere models are solely based  
424 on temperatures in the preceding months<sup>44-45</sup>. We determined the length of the preseason  
425 whose average  $T_{\text{day}}$  had the most influence on LSD by calculating the partial correlation  
426 coefficients between LSD and mean  $T_{\text{day}}$  during 0, 1, 2, ...  $n$  months prior to LSD,  
427 controlling for corresponding mean  $T_{\text{night}}$ , total precipitation, and radiation. The maximum  
428 range ( $n$ ) of the preseason is generally from June to the multiyear mean date of LSD (see  
429 Fig. S20 for example). The partial correlation coefficients with the highest absolute values  
430 were then used in the following analysis. We obtained the relationship between LSD and  
431  $T_{\text{night}}$  the same way but replacing  $T_{\text{day}}$  with  $T_{\text{night}}$ . This analytical procedure was applied for  
432 observed LSD from ground sites and derived LSD from the MODIS and GIMMS NDVI3g  
433 data.

434

## 435 **5. Models for predicting LSD**

436 Our results indicated that LSD responded oppositely to  $T_{day}$  and  $T_{night}$ , so we  
 437 developed a weighted day-night-temperature growing-degree-day ( $DN_{GDD}$ ) algorithm from  
 438 observations to model LSD, and compared the algorithm with currently used threshold  
 439 and GDD models based on  $T_{mean}$ <sup>46</sup>.

440 The threshold model was the simplest method. We calculated average  $T_{mean}$  for five  
 441 days before LSD in each year and used the multiyear mean value as the threshold to  
 442 model LSD. If  $T_{mean}$  was lower than the threshold for five consecutive days from 1st July,  
 443 the last date was considered the LSD.

444 GDD was calculated as:

$$445 \quad GDD(d) = \max(T_b - T_{mean}(d), 0) \quad (3)$$

$$446 \quad GDD_{threshold} = \sum_{d=d_0}^{LCD} GDD(d) \quad (4)$$

447 where  $T_b$  is the base temperature set to 15, 20, 25, and 30 °C,  $T_{mean}(d)$  is the mean  
 448 daily temperature, and  $d_0$  is the date on which the calculation begins (1st July in this  
 449 study). LSD is the observed or derived date of leaf coloring in each year. The date when  
 450  $GDD(d)$  exceeded the multiyear average GDD threshold was defined as LSD.

451 Our  $DN_{GDD}$  model improved upon the original GDD model and was calculated by:

$$452 \quad GDD(d) = k \cdot \max(T_b - T_{day}(d), 0) + (1 - k) \cdot \max(T_b - T_{night}(d), 0) \quad (5)$$

453 where  $T_{day}(d)$  is the daily maximum temperature,  $T_{night}(d)$  is the daily minimum  
 454 temperature, and  $k$  is the weighting factor. When  $0 < k < 1$ , the effects of  $T_{day}$  and  $T_{night}$  on  
 455 LSD are consistently positive; When  $k > 1$  or  $k < 0$ , the effects of  $T_{day}$  and  $T_{night}$  on LSD are  
 456 opposite. In order to determine the value of  $k$ , we first calculated the ratio of  $R_{day}$  and  $R_{night}$   
 457 for each station or pixel, and found 99.9% of the ratio values were between -10 and 10 for

458 both ground and satellite data (Figure S21). In other words, the level of  $T_{\text{day}}(T_{\text{night}})$  effect  
459 could be 1 to 10 times than the level of  $T_{\text{night}}(T_{\text{day}})$  effect (note that  $T_{\text{day}}$  represents  $T_{\text{day}}$  with  
460 the effects of  $T_{\text{night}}$  removed). Therefore, the values of  $k$  ranged from  $-1$  to  $2$  (see Table  
461 S3). In addition, when  $k$  tends to infinity, the effects of  $T_{\text{day}}$  and  $T_{\text{night}}$  on LSD are opposite  
462 with same level.

463 We evaluated the accuracy and obtained the most appropriate parameters of the  
464 models by calculating the correlation coefficient ( $R$ ) and the root mean square error  
465 (RMSE) between modeled and observed LSD.  $T_b$  and  $k$  with the lowest RMSE were  
466 considered the most appropriate values for each site or pixel.

467

#### 468 **Data Availability**

469 The data that support the findings of this study are available from the corresponding  
470 author upon request.

471

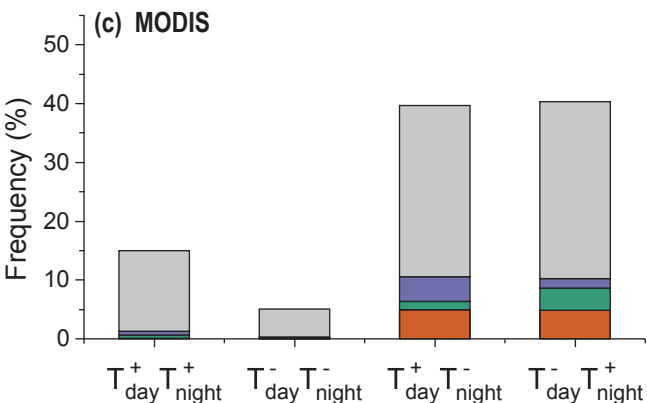
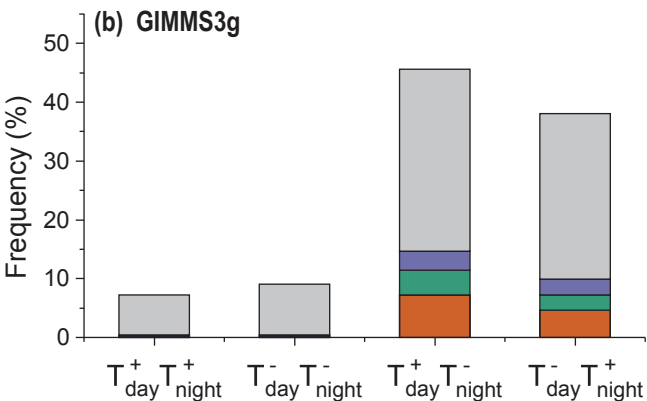
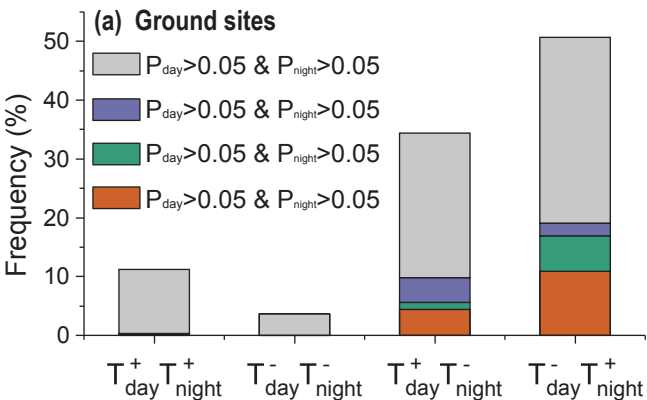
#### 472 **References**

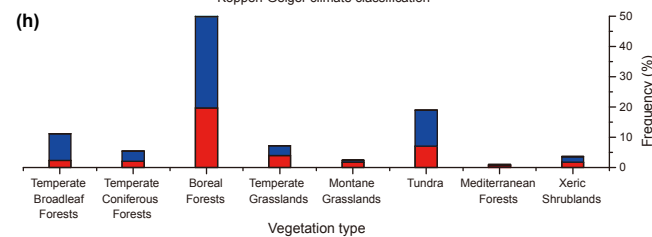
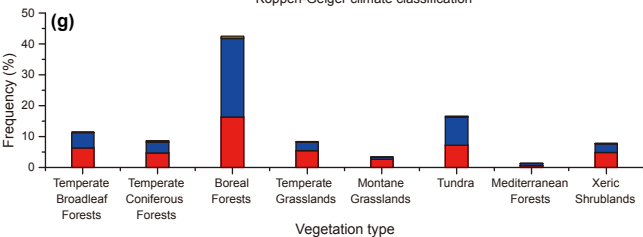
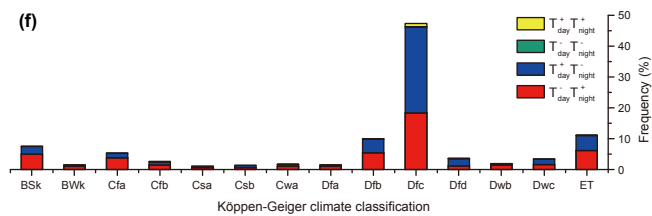
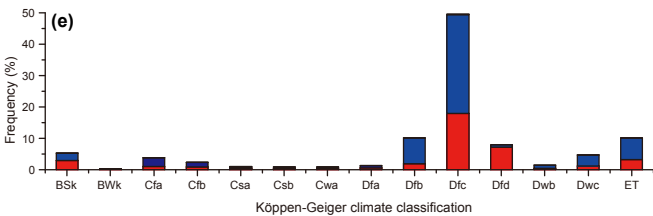
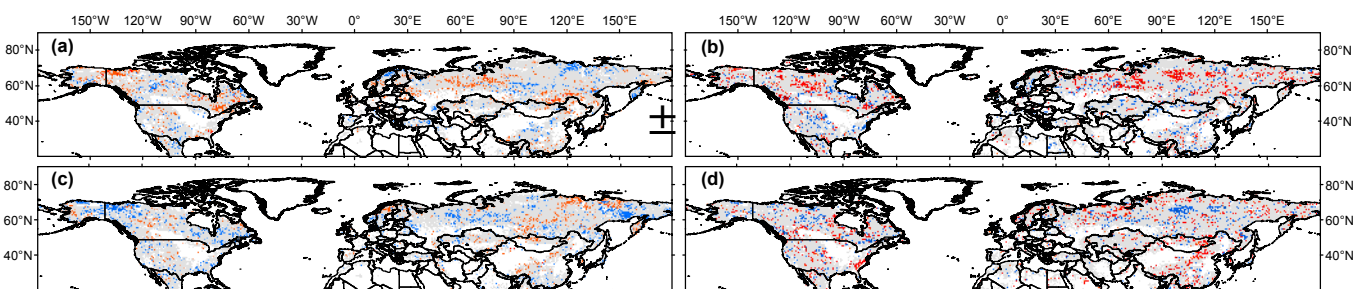
- 473 31. Park, C.K., et al., (2017). Spatial and temporal changes in leaf coloring date of *Acer*  
474 *palmatum* and *Ginkgo biloba* in response to temperature increases in South Korea.  
475 PLoS ONE, 12.
- 476 32. Schaber, J., & Badeck, F.W. (2002). Evaluation of methods for the combination of  
477 phenological time series and outlier detection. *Tree Physiology*, 22, 973-982.
- 478 33. Huete, A., et al., (2002). Overview of the radiometric and biophysical performance of  
479 the MODIS vegetation indices. *Remote sensing of environment*, 83, 195-213.

- 480 34. Zhang, X., et al. (2003). Monitoring vegetation phenology using MODIS. Remote  
481 sensing of environment, 84, 471-475.
- 482 35. Shen, M., et al., (2014). Increasing altitudinal gradient of spring vegetation phenology  
483 during the last decade on the Qinghai–Tibetan Plateau. Agricultural and Forest  
484 Meteorology, 189, 71-80.
- 485 36. Chen, J., et al., (2004). A simple method for reconstructing a high-quality NDVI  
486 time-series data set based on the Savitzky–Golay filter. Remote sensing of  
487 environment, 91, 332-344.
- 488 37. Piao, S., et al., (2011). Changes in satellite-derived vegetation growth trend in  
489 temperate and boreal Eurasia from 1982 to 2006. Global Change Biology, 17,  
490 3228-3239.
- 491 38. White, M.A., et al. (1997). A continental phenology model for monitoring vegetation  
492 responses to interannual climatic variability. Global Biogeochemical Cycles, 11,  
493 217-234.
- 494 39. Elmore, A.J., et al., (2012). Landscape controls on the timing of spring, autumn, and  
495 growing season length in mid-Atlantic forests. Global Change Biology, 18,  
496 656-674.
- 497 40. Olson, D. M., et al. (2001). Terrestrial ecoregions of the world: a new map of life on  
498 earth. Bioscience, 51, 933-938.
- 499 41. Zeng, H., & Jia, G. (2013). Impacts of snow cover on vegetation phenology in the  
500 arctic from satellite data. Advances in Atmospheric Sciences, 30, 1421-1432.
- 501 42. Wang, X. et al. 2018. Snow cover phenology affects alpine vegetation growth

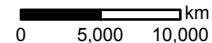
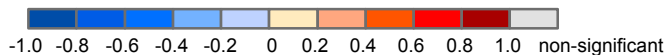


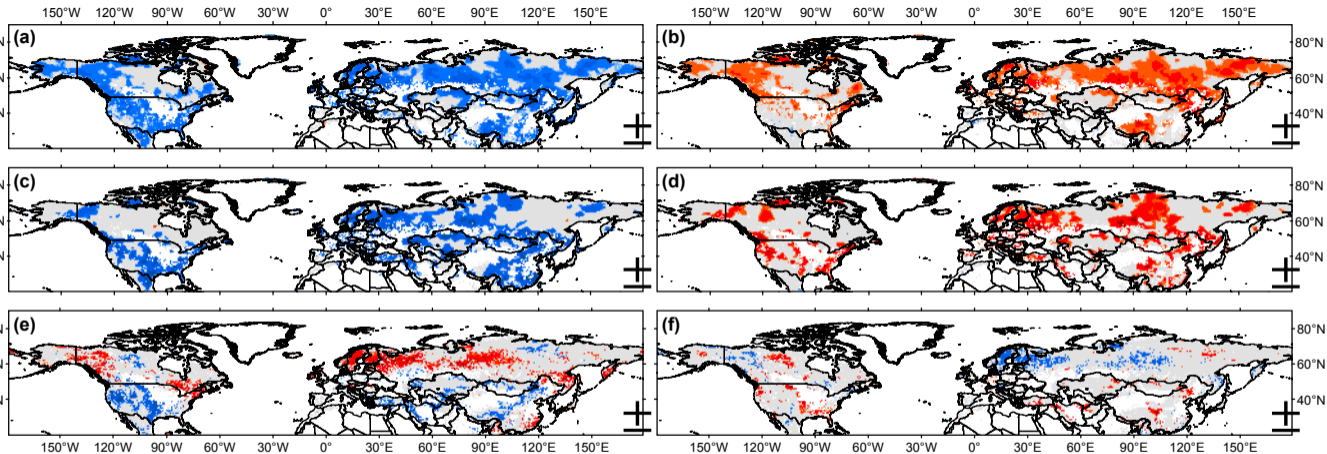
- 502 dynamics on the Tibetan Plateau: Satellite observed evidence, impacts of biomes,  
503 and climate drivers. *Agricultural and Forest Meteorology*, 256, 61-74.
- 504 43. Silva, A. A., & Echer, M. P. D. S. (2013). Ground-based measurements of local cloud  
505 cover. *Meteorology & Atmospheric Physics*, 120, 201-212.
- 506 44. Delpierre, N., et al. (2009). Modelling interannual and spatial variability of leaf  
507 senescence for three deciduous tree species in france. *Agricultural & Forest*  
508 *Meteorology*, 149, 938-948.
- 509 45. Richardson, A.D., et al., (2012). Terrestrial biosphere models need better  
510 representation of vegetation phenology: results from the North American Carbon  
511 Program Site Synthesis. *Global Change Biology*, 18, 566-584.
- 512 46. Krinner, G., et al., (2005). A dynamic global vegetation model for studies of the  
513 coupled atmosphere-biosphere system. *Global Biogeochemical Cycles*, 19,  
514 doi:10.1029/2003GB002199.





Partial correlation coefficient





Partial correlation coefficient

